DOI: 10.1002/adfm.200500429

Electrical Switching and Bistability in Organic/Polymeric Thin Films and Memory Devices**

By *Yang Yang*,* *Jianyong Ouyang*, *Liping Ma*, *Ricky Jia-Hung Tseng*, and *Chih-Wei Chu*

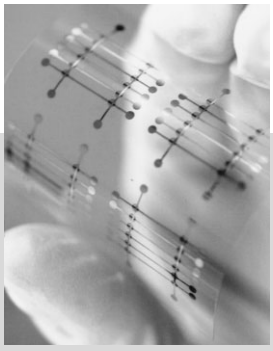

Recently, films created by incorporating metallic nanoparticles into organic or polymeric materials have demonstrated electrical bistability, as well as the memory effect, when subjected to an electrical bias. Organic and polymeric digital memory devices based on this bistable electronic behavior have emerged as a viable technology in the field of organic electronics. These devices exhibit fast response speeds and can form multiple-layer stacking structures, demonstrating that organic memory devices possess a high potential to become flexible, ultrafast, and ultrahigh-density memory devices. This behavior is believed to be related to charge storage in the organic or polymer film, where devices are able to exhibit two different states of conductivity often separated by several orders of magnitude. By defining the two states as "1" and "0", it is now possible to create digital memory devices with this technology. This article reviews electrically bistable devices developed in our laboratory. Our research has stimulated strong interest in this area worldwide. The research by other laboratories is reviewed as well.

1. Introduction

Organic materials have attracted a lot of attention for building large-area, mechanically flexible electronic devices.[1] Organic light-emitting diodes for flat-panel displays are ready for mass production,[2] and significant progress has also been made in organic thin-film transistors,[3] and organic solar cells.[4] There is a strong desire to develop new advanced materials that can overcome the potentially limiting scaling difficulties present in the semiconductor industry. Development of future information technology could come from data storage incorporating these advanced materials. So far, many methods have been reported for achieving inorganic nonvolatile memory, such as implementing phase-change memory,[5] programmable metallization cells,[6] mechanical switches,[7] quantized atomic switches,[8] quantum dots,[9] and nanocrystal memory.[10]

Organic materials are promising candidates for electronic devices in new information technologies.[11] The devices can be fabricated through either a bottom–up method or by forming a composite active layer, and can be easily addressed by *x*–*y* cross-wire, two-terminal structures, which sandwich the active layer. The use of organic materials provides a simplified manufacturing process yielding low-cost, flexible, and light-weight devices that have an active device area approaching the nanoscale. To examine the processibility of these devices while scaling to the nanoscale, some experiments were conducted using scanning tunneling microscopy[12] and cross-wired junctions.[12a,13] In general, the memory effect observed in these organic devices is related to charge storage (including charge trapping, charge separation, and change transfer)[14,15] within active components in the organic layer. The critical material requirement for the memory effect is the existence of an energy barrier preventing the positive and negative charges from recombining, even after the electric bias has been removed.

[*] Prof. Y. Yang, Dr. J. Ouyang, Dr. L. Ma, R. J.-H. Tseng, C.-W. Chu
Department of Materials Science and Engineering
University of California, Los Angeles
Los Angeles, CA 90095 (USA)
E-mail: yangy@ucla.edu

[**] The authors thank Prof. Richard Kaner of the Chemistry Department of UCLA for his collaboration and providing the PANI nanofiber. Technical discussions with Dr. Chuck Szmanda of Rohm Haas, Prof. Qibing Pei of UCLA, and Dr. Ed Chandras of Bell Labs are also acknowledged. We are indebted to Mr. Brian Shedd for his help in polishing our English. Finally, we express ultimate thanks to our financial supporters over the past several years on the organic/polymeric memory devices. The Office of Naval Research and National Science Foundation provided the initial funds for the triple-layer organic memory devices. The Air Force of Scientific Research provided the funding for the polymer memory devices. Finally, the PANI/Au NP memory device was supported by the UCLA FENA-MACRO Center with funds from the Semiconductor Research Corporation (SRC) and the Defense Advanced Research Project Agency (DARPA).

After the materials have been polarized, the device exhibits a conductance change, where a low-conductance (OFF) state switches to a high-conductance (ON) state, resulting in so-called electrically bistable devices. The states are stable for prolonged periods of time, allowing them to be used in nonvolatile memory device applications, such as flash memory and random access memory. In addition to memory applications, organic electronic devices have also demonstrated the potential to be used as switches to drive organic light-emitting diodes for electronic-display applications.[16] This article covers memory devices incorporating a two-terminal structure and an active thin film sandwiched between two electrodes. It does not include devices using single or multiple molecular layers, or devices with a three-terminal structure.[17]

Organic memory devices and organic logic circuits are often characterized by their reliability. The nonvolatile performance criteria that must be satisfied for a device to be considered reliable are data retention for at least ten years, low power consumption, and 10^6 operation cycles. These criteria are comparable to those provided by flash memory. Here, we introduce several organic materials and device structures that show promise for memory applications, while also analyzing their bistability mechanisms, retention times, cycling tests, and overall operation. Nevertheless, the technology at this stage has not yet matured, so hopefully we can encourage and provide motivation for further research in this area to provide future technology for memory applications.

Our laboratory pioneered the development of organic or polymer bistable devices. In this article, we review five types of bistable devices developed at our laboratory. The first device has the architecture of a triple layer (organic/metal-nanocluster/organic (OMO)) sandwiched between two metal electrodes and is presented in Section 2. The other four devices have the architecture of a single layer sandwiched between two metal electrodes. The active layer of these devices is a polymer film containing different materials. The second device presented in this article uses polymer/metal nanoparticles (NPs) in the active layer and is discussed in Section 3. The devices with three different materials systems are presented in Section 4. Our research stimulated strong interest in this area worldwide. The research by other laboratories is reviewed in Section 5.

2. Triple-Layer Device Fabricated via Thermal Evaporation

The device with a triple-layer structure sandwiched between two metal electrodes is introduced in this section. The chemical structure of some materials presented in this and the following sections are listed in Figure 1. The material layers of these devices are deposited by thermal evaporation, so it is imperative that this process is accurately controlled in order to generate functional devices. Material selection is critical to this process, as only the correct combination of materials will create the desired memory effect. Here, the fabrication procedures are discussed and device operation is analyzed. The resulting memory performance is evaluated based on retention time and write–read–erase cycles of the devices. This information also allows further conclusions to be drawn regarding the device-switching mechanism.

2.1. Device Fabrication

The active layer of the organic bistable device (OBD) consists of a nominal organic/metal-nanocluster/organic trilayer structure interposed between an anode and a cathode, as shown in the bottom inset of Figure 2.[18b] Thus, the entire device structure is given as Al/OMO/Al. A photo of a typical device is shown in the top inset of Figure 2. Initially 2-amino-4,5-imidazoledicarbonitrile (AIDCN) was selected for the organic material and Al was used for the middle metal layer and the top and bottom electrodes. However, various other materials have been used to fabricate functional devices. As mentioned earlier, the material layers were deposited by several sequential thermal evaporations under a vacuum of 1×10^{-6} Torr (1 Torr = 133.32 Pa) without ever breaking the vacuum. It is important to note that a pure metallic middle layer leads to a nonfunctional device, so the formation of metal nanoclusters is critical to achieving the memory effect. During the evaporation of the middle Al-nanocluster layer, a small amount of AIDCN vapor was purposely introduced to obtain more controllable device-fabrication conditions, yielding a unique co-evaporation process of Al and AIDCN. By carefully adjusting the Al/

Yang Yang is a professor in the Department of Materials Science and Engineering at the University of California, Los Angeles. Yang obtained his Ph.D. degree in Physics and Applied Physics at the University of Massachusetts Lowell in 1992, under the supervision of Professor Jayant Kumar and the late Professor Sukant K. Tripathy. Yang's research focuses on conjugated organics and polymer materials and devices, such as light-emitting diodes, memory devices, transistors, and solar cells. He has published more than 100 refereed papers, given more than 50 invited presentations on his research work, and has filed or been granted 22 US patents. Currently, Yang's group has five post-docs/visiting scholars, and 15 students. He has received the Outstanding Overseas Young Chinese Scientist Award from the Natural Science Foundation of China (2004), the NSF Career Award (1998), and the 3M Young Investigator Funds (1998). Yang serves on boards of several companies and government committees. He is a co-founder of ORFID Corporation, a start-up company located in Los Angeles focusing on organic transistors for displays and organic RFID.

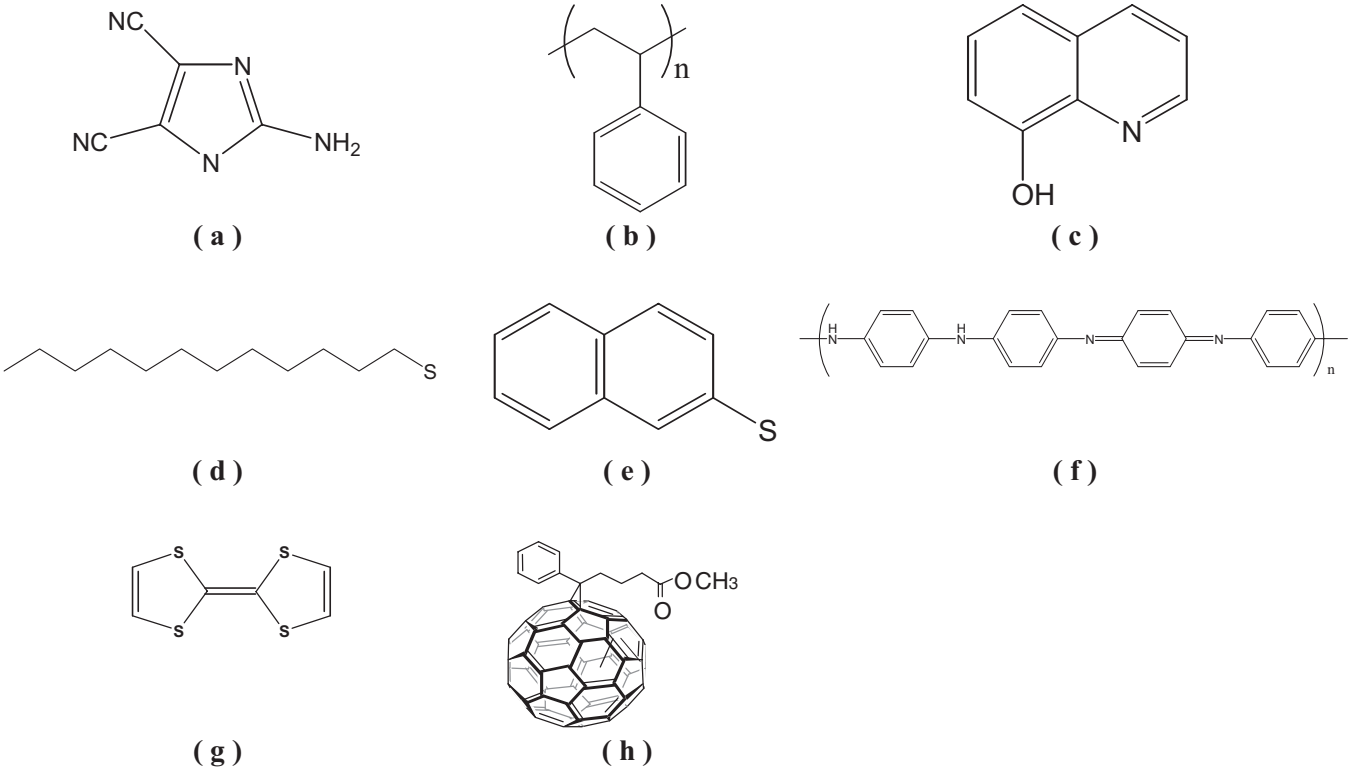

Figure 1. Chemical structures of a) 2-amino-4,5-imidazoledicarbonitrile (AIDCN), b) polystyrene (PS), c) 8-hydroxyquinoline (8HQ), d) 1-dodecanethiol (DT), e) 2-naphthalenethiol (2NT), f) polyaniline (PANI), g) tetrathiafulvalene (TTF), and h) [6,6]-phenyl C_{61}-butyric acid methyl ester (PCBM).

AIDCN volume ratio, it was determined that the optimum ratio of Al/AIDCN for the formation of the Al-nanocluster layer in the chamber is 3:1 to 4:1, where the device yield is over 95 % percent. (This ratio may vary in different chambers.)

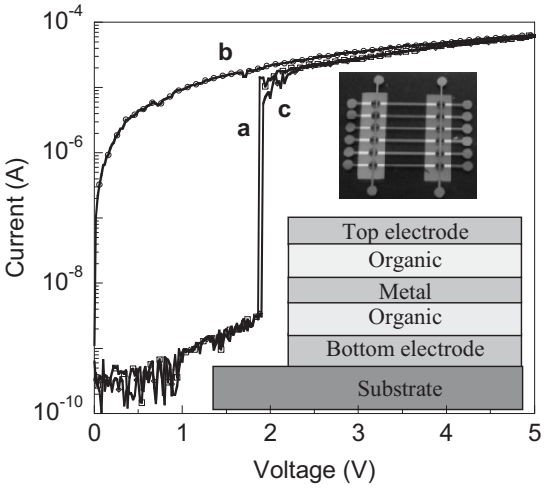

Figure 2. Current–voltage (*I–V*) curves of an OBD with the nominal structure Al/AIDCN (50 nm)/Al nanoclusters (20 nm)/AIDCN (50 nm)/Al. Curves (a,b) represent the *I–V* characteristics of the first and second bias scan, respectively. Curve (c) is the *I–V* curve of the third bias scan after the application of a reverse voltage pulse (–3 V). The bottom inset shows the device structure, the top inset shows an image of a typical OBD. Reproduced with permission from [18b]. Copyright 2002, American Institute of Physics.

Atomic force microscopy (AFM) images of the surface of the Al/AIDCN layer with a ratio of 3.3:1 indicate a metal–organic nanocomposite structure, as shown in Figure 3.[19] Further analysis of the nanoclusters shows that they each consist of a metallic core and an aluminum oxide shell, which results from the reaction of Al with AIDCN and/or oxygen during the co-evaporation process. Thus, a very thin oxidation layer between the metallic Al nanoclusters is formed. More details about the device fabrication can also be found in the literature.[18]

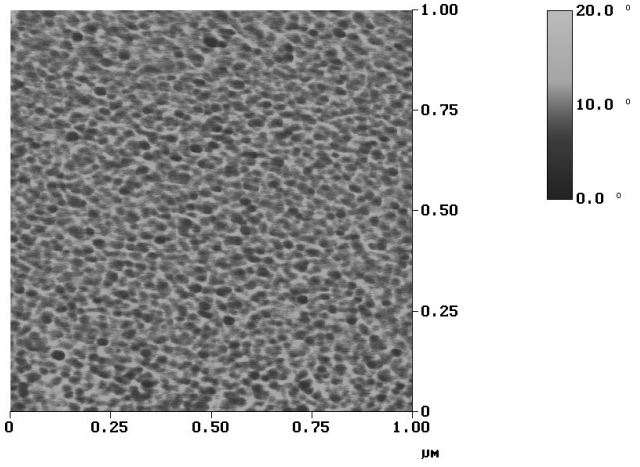

Figure 3. AFM phase image of the surface of an Al/AIDCN (3.3:1) layer. Reproduced with permission from [19]. Copyright 2004, the MRS Bulletin.

2.2. Electrical Characteristics

A typical current–voltage (*I–V*) curve for an OBD is shown in Figure 2. The first voltage scan, depicted by curve a, shows a sharp increase in the current at about 2 V. After this transition, the device remains in this high-current state even after turning off the power. This can be seen in the second voltage scan (curve b) in Figure 2. Curve c in Figure 2 shows the *I–V* characteristics of the device after the application of a –3 V bias; it is nearly identical to curve a.

The estimated electron travel time from the electrode to the middle layer would be about 1 μs, which is based on an AIDCN layer with a thickness of 50 nm and a charge mobility of 10^{-5} $cm^2 V^{-1} s^{-1}$. However, the switching time for the OBDs is actually less than 20 ns, as seen in the inset of Figure 4.[18b] This nanosecond response time suggests that the electrical-switching process is probably not caused by a simple charge-trapping process, which is defined by charge injection from the electrode, electron transportation through the medium, and charge trapping within the metal-nanoclusters layer, but rather a field-induced effect. Furthermore, the switching voltage of the OBDs is independent of the temperature (Fig. 4),[20] which suggests that a tunneling process is veritably responsible for the switching process, rather than a process flow comprised of charge injection, transportation, and trapping, which has a strong dependence on temperature.

The memory retention of these devices was evaluated by leaving several OBDs in the ON state at ambient conditions and monitoring the current. It was found that the devices remain in the ON state for several days to weeks. The origin of the variation in the retention ability is still under investigation. The devices exemplify good rewritable characteristics during cycle testing (shown in Fig. 5), where more than one million write–read–erase cycles were performed on the OBD without failure.

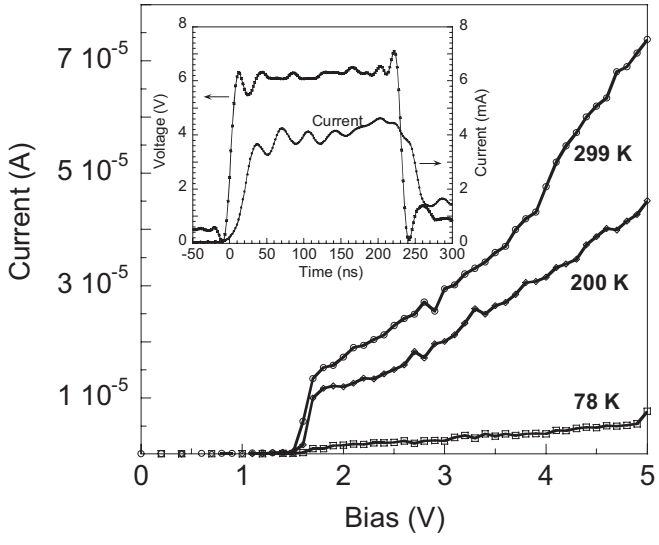

Figure 4. *I–V* curves of an OBD at various temperatures. The inset shows the dynamic response of an OBD initially in the OFF state to an applied voltage pulse. Reproduced with permission from [20]. Copyright 2002, Taylor & Francis.

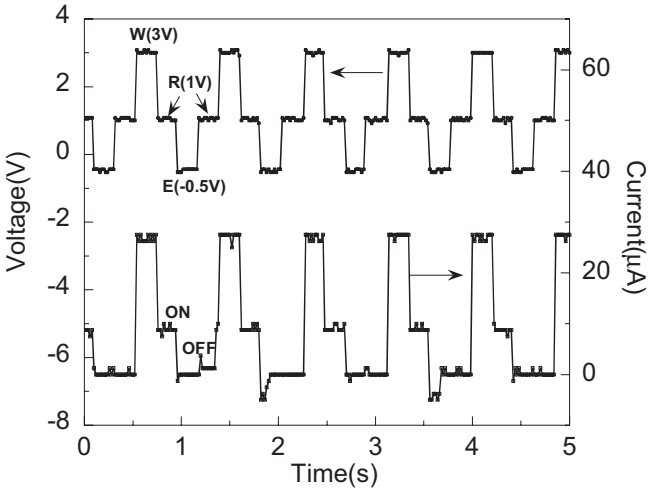

Figure 5. Typical current responses of an OBD during the write–read–erase voltage cycle. Reproduced with permission from [18b]. Copyright 2002, American Institute of Physics.

2.3. Conduction and Switching Mechanisms

The energy diagram of the unbiased Al-nanocluster layer shows a distribution of many energy wells (nanoclusters) next to each other, which are sandwiched between the two organic layers with relatively high LUMO–HOMO (lowest unoccupied molecular orbital–highest occupied molecular orbital) energy levels. When a sufficient bias is applied to the device, the Al-nanocluster layer becomes polarized, and opposite charges are subsequently induced (or stored) at the top and bottom interfaces of the middle Al-nanocluster layer and organic layers. The stored charges lower the interfacial resistance and switch the device to the ON state, while only a reverse bias can restore the device to the OFF state. In this fashion, a nonvolatile-memory effect is created. The charge storage in our OBD device comes from the redistribution of charges within the partially oxidized Al-nanocluster layer; hence, the switching process is very fast, which is demonstrated by the write speed of the devices being in the nanosecond regime. Further, the oxide layer between the metal nanoclusters prevents charge recombination after the voltage is removed.

We have established a theoretical model using the single-band Hubbard model[21] that considers the interactions among the nanoclusters, organic molecules, and electrodes.[22] Initially the electron-transmission probability is calculated for the devices in two generalized situations. The first situation represents the case where no charge is stored in the metal nanoclusters, and the other situation considers the case where positive/negative charges are stored on both sides of the nanocluster layer, as shown in the insets of Figure 6. It was found that the electron transmission probability increases by several orders of

ADVANCED FUNCTIONAL MATERIALS

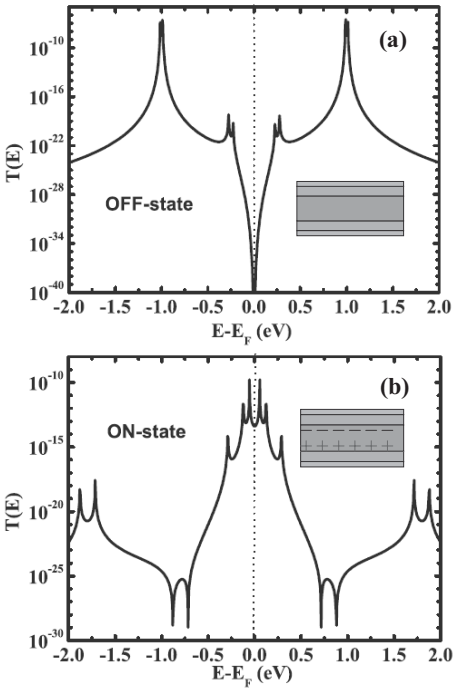

Figure 6. The transmission probabilities $T(E)$ as a function of energy for the following cases: a) without charges in the nanocluster layer, and b) with positive/negative charges stored in the nanocluster layer. The insets show the corresponding device states. Reproduced with permission from [22]. Copyright 2004, the American Physical Society.

magnitude when the metal-nanocluster layer is positively/negatively charged, which is in agreement with the OBD-operation mechanism.

In order to further examine the potential difference across the active interfaces of the device, the middle nanocluster layer was externally wired to measure the potential change across only one interface. A potential difference between the middle nanocluster layer and the bottom electrode was measured, and the conductivity was shown to change by more than three orders of magnitude between the OFF and ON states.[23] This directly proves our proposal that device switching is a result of charge storage at the interface of the nanocluster/organic layer.

3. Polymer/NP Version of the Single-Layer Device

The organic memory device has made a giant leap in technology by simplifying the layered structure into a single-layer polymer memory device, which can be formed by solution processing. In this section, nonvolatile memory is demonstrated using a polymer film blended with small conjugated organic compounds and metal NPs.[24,25] The metal NPs are capped with saturated alkanethiols, and this device has a very simple architecture—essentially just a polymer film sandwiched between two metal electrodes.

3.1. Device Fabrication

The device layout is shown in Figure 7. The gold NPs, prepared by the two-phase arrested growth method,[26] are capped with 1-dodecanethiol (DT) (hereafter referred to as Au–DT NPs) and have a narrow size distribution (1.6–4.4 nm in diameter) and an average particle size of 2.8 nm. For fabrication, at first the bottom Al electrode was thermally evaporated onto a glass substrate in a very clean chamber at a vacuum pressure of 10^{-5} Torr. Next, the active layer was formed by spin-coating a solution of 0.4 wt % Au–DT NPs, 0.4 wt % 8-hydroxyquinoline (8HQ), and 1.2 wt % polystyrene (PS) in 1,2-dichlorobenzene. The polymer film had a thickness of about 50 nm. Finally, the device was completed by thermal evaporation of the top Al electrode. The top and bottom Al electrodes had line widths of 0.2 mm and were aligned perpendicular to each other, so that the device had an area of 0.04 mm^2 (0.2 mm × 0.2 mm). This device is represented as Al/Au–DT NP + 8HQ + PS/Al in this manuscript.

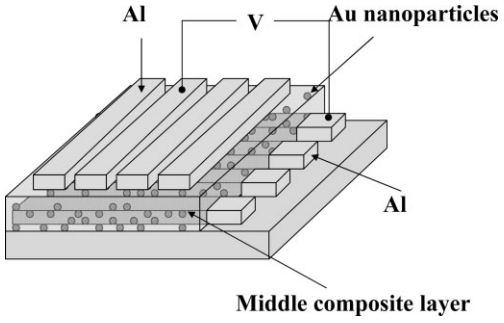

Figure 7. Device structure of polymer memory device.

3.2. Electrical Characteristics

The I–V curves for the Al/Au–DT NP + 8HQ + PS/Al system is shown in Figure 8. This pristine device exhibited a very low current, approximately 10^{-11} A at 1 V. The electrical transition from the low- to the high-conductivity state took place at 2.8 V

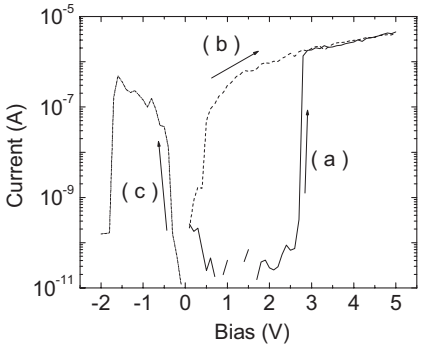

Figure 8. I–V curve of an Al/Au–DT NP + 8HQ + PS/Al device tested in vacuum: a) first, b) second, and c) third bias scans. The arrows indicate the voltage-scanning directions. Reproduced with permission from [24]. Copyright 2004, the Nature Publishing Group.

with a dramatic current increase from 10^{-11} to 10^{-6} A (curve a). The high-conductivity state is able to return to the low-conductivity state by applying a negative bias as indicated in curve c, where the current suddenly dropped to 10^{-10} A at –1.7 V.

The device exhibited similar behavior when it was tested in a nitrogen atmosphere and also in air. The transition voltage and current for the device in the high-conductivity state are almost the same as for the device tested in vacuum, while the current for the device in the low-conductivity state tested in air is higher by one to two orders of magnitude than for that tested in vacuum. These responses indicate that oxygen and moisture do not have a significant effect on the electrical transitions.

Cycling between the high- and low-conductivity states of the device was performed numerous times in air. The write, read, and erase voltages used for the cycle tests were 5, 1.1, and –2.3 V, respectively. After applying a pulse of 5 V for a duration of 25 ns, the current became four orders of magnitude higher. Currently, our equipment (HP 214B Pulse Generator) is incapable of generating a pulse shorter than 25 ns, so it is therefore possible that the response time of this device is actually faster than what we are able to measure.

To study the impact of material composition on device performance, other materials were also used to fabricate the device. For example, when 8HQ was replaced by other conjugated organic compounds (such as 9,10-dimethylanthracene) and PS was replaced by poly(methyl methacrylate) (PMMA), similar electrical behavior to that obtained in the initial case was observed. However, when a PMMA film consisting of only Au–DT NPs without 8HQ or any other conjugated organic compound was used, no remarkable electrical switching was observed. Another material-related concern, potentially harmful to proper device operation, is the possible oxidation of the Al electrodes. To test whether this is a viable concern that could affect device performance, devices using other conductive materials, such as Au, copper, and indium tin oxide (ITO), as one or both electrodes were also fabricated. Since these devices exhibited quite similar electrical behavior to the device using Al as both electrodes, it can be concluded that a very thin aluminum oxide layer at the electrode interface did not affect the electrical transition. Moreover, the operation of the device can be combined with AFM, so that an extremely high device density can be achieved. (Results in a previous publication.[24])

3.3. Conduction and Switching Mechanisms

The nanosecond-scale transition of these devices and the electric-field-induced change of the surface potential of the polymer film both indicate that the switching process may be an electronic one rather than one involving chemical rearrangement, conformational change, or isomerization. For example, conformational change for a ferroelectric polymer occurs on a 30 μs time scale.[27] Atomic movement or molecular isomerization that can result in electrical bistability was observed on molecular devices;[28,29] however, the transition time was on the order of milliseconds and in some cases even longer.

To further study the switching mechanism we employed ac–impedance spectroscopy, which allows the study of energy levels and transport mechanisms of materials. Our experimental results suggest that the switching mechanism is not due to the formation of conductive filaments[30] between the two metal electrodes, which is observed in other polymer-film systems.[31] It is unlikely that filament formation is the reason for the electronic transitions in our device, since the electrical behavior of our device is strongly dependent on the structure and the concentration of the gold NPs. In addition, ac-impedance studies from 20 to 10^6 Hz indicate that the electronic transitions in our device are different from the dielectric breakdown found in polymer films. (Results presented in a previous publication.[25]) We observed dielectric breakdown in devices with a PS film sandwiched between two Al electrodes where, after breakdown, the current increased by more than four orders of magnitude and the capacitance was lowered by about one order of magnitude across the whole frequency range. In comparison, the Al/Au–DT NPs + 8HQ + PS/Al system exhibited an increase in current by more than four orders of magnitude. When the device was in the high-conductivity state, the capacitance increased in the low-frequency range, while it remained the same in the high-frequency range. These studies suggest that space charges may generate in the film after the as-prepared device is electrically switched to a high-conductivity state. PS may act merely as an inert matrix for Au–DT NPs and 8HQ, and, as a result, will not play a role in the electronic transition mechanism.

The conduction mechanism for Al/Au–DT NPs + 8HQ + PS/Al in the low-conductivity state may be due to a small amount of impurity present in the active layer or through hot-electron injection. The conduction mechanism of the device in the high-conductivity state was studied by the temperature dependence of the current and analysis of the *I–V* behavior. (Results presented in a previous publication.[24]) The current for the device in the high-conductivity state was almost temperature-independent, and the *I–V* curves can be accurately fit by a combination of direct tunneling (tunneling through a square barrier) and Fowler–Nordheim tunneling (tunneling through a triangular barrier), as given by the following expression:[32]

$$I = C_1 V \mathrm{e}^{-\frac{2d\sqrt{2m^*\Phi}}{\hbar}} + C_2 V^2 \mathrm{e}^{-\frac{4d\Phi^{3/2}\sqrt{2m^*}}{3q\hbar V}} \quad (1)$$

The first term on the right hand side of the equation is the current contributed by direct tunneling, and the second term is the current contributed by Fowler–Nordheim tunneling. In this equation, d is the tunneling distance, m^* is the effective mass of the charge carrier, C_1, C_2 are constants, e is the base of the natural logarithm, $\hbar = h/2\pi$, where h is Planck's constant, q is the electronic charge, and Φ is the energy-barrier height. At low voltage ($V < \Phi$), direct tunneling is the dominant conduction mechanism, and at high voltage ($V > \Phi$), Fowler– Nordheim tunneling becomes the dominant conduction mechanism.

The different conduction mechanisms in the two states suggest that a change occurs in the electronic structure of the device after the electrical transition. It has already been demonstrated that 8HQ and gold NPs can act as electron donors[33]

ADVANCED FUNCTIONAL MATERIALS

and acceptors,[34] respectively. Moreover, the different surface potentials of the Au–DT NPs + 8HQ + PS film after treatment with different electric fields suggest that the electric field can induce polarization of the film. Hence, we propose a charge-transfer effect occurring between the Au–DT NPs and 8HQ under a high electric field that results in electronic transition. Prior to the electronic transition there is no interaction between the Au–DT NPs and 8HQ and, since the concentration of charge carriers due to impurities in the film is quite low, the film initially exhibits very low conductivity. However, when the electrical field increases to a certain value, electrons on the HOMO of 8HQ may gain enough energy to tunnel through the capping molecule, DT, and into the gold NP (Fig. 9a). Consequently, the HOMO of 8HQ becomes partially filled, so that 8HQ and the gold NPs are positively and negatively charged, respectively. Carriers are then generated and the device is able to switch to a high-conductivity state after the charge transfer. This phenomenon is presupposed though, as it is well known that the conductivity of conjugated organic compounds will increase after their HOMO or LUMO becomes partially filled.[16,35]

Considering the case for an electrical transition leads to closer analysis of the electrically active materials within the system. Since the separation between 8HQ molecules in the polymer film will be larger than that in the 8HQ crystal (a simple estimation suggests that the separation between the 8HQ molecules in the Au–DT NP + 8HQ + PS film is about 6 to 10 Å), it is reasonable that tunneling becomes the dominant charge-transport mechanism among the 8HQ molecules.

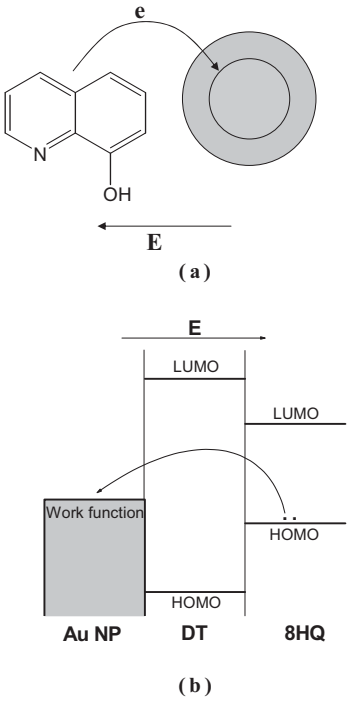

Figure 9. a) Schematic of the electron transfer from 8HQ to the core of the gold NP. The inner gray circle indicates the core of the gold NP, and the outer gray ring indicates the capped DT. b) Energy-level diagram of the core of the gold NP, DT, and 8HQ. The two dots on the HOMO of 8HQ represent two electrons. The straight arrow indicates the direction of the electric field (*E*), and the curved arrow indicates the electron transfer from 8HQ to the core of the gold NP. Reproduced with permission from [25]. Copyright 2005, IEEE.

Stability of the negative charge on the gold NPs is due to the insulating coating on the gold NPs (DT), which prevents recombination of the charge after removal of the external electric field. Since an external electrical field induces the charge transfer, the film becomes polarized after the charge transfer, and only a reverse electric field can cause tunneling of the electron from the gold NP back to the HOMO of $8HQ^+$, resulting in a return to the low-conductivity state. Charge tunneling through the insulator coating on the gold NP is possible, and it has been observed frequently that gold NPs coated with an insulating alkanethiol layer can be reduced or oxidized through electrochemical methods.[36]

The HOMO and LUMO levels of 8HQ, calculated by means of density functional theory using Becke's three-parameter functional with the Lee, Yang, and Lee correlation functional (DFT B3LYP) method with the 6-31+G(d,p) basis set,[37] are 1.9 and 6.1 eV, respectively (Fig. 9b). The quantized energy, δ, for a gold NP with a diameter of 2.8 nm is about 0.014 eV calculated using the following equation:[38]

$$\delta = \frac{4E_F}{3N} \tag{2}$$

where E_F is the Fermi energy of bulk Au, and N denotes the number of Au atoms in one gold NP. This quantized energy is even much smaller than the thermal energy at room temperature, so that its effect can be neglected. On the other hand, the Coulomb energy (E_c) needed to charge a gold NP with a diameter of 2.8 nm capped with DT is about 0.1 eV, as calculated using the equations[39]

$$E_c = \frac{e^2}{2C} \tag{3}$$

and

$$C = 4\pi\varepsilon_0\varepsilon_r \frac{r}{d}(r+d) \tag{4}$$

where C is the capacitance of the gold NP, ε_0 the permittivity of free space, ε_r the permittivity of the capped molecule on the gold NP, r the radius of the gold NP core, and d the length of the capped molecule. This charging energy is the energy to be overcome for the charge transfer to take place. It is possible for the electron to gain such energy under a high electric field. These considerations on the energies suggest that charge transfer from 8HQ to gold NP is possible under the application of a high electric field. This electric-field-induced charge-transfer model explains the electronic transition observed in the Al/Au–DT NP + 8HQ + PS/Al system quite well, and is supported by the evidence noted above.

4. Advanced Memory Device Architectures with a Single-Layer Structure

Based on our understanding of the field-induced switching mechanism, several material systems have been developed that

either generate additional functionality or simplify the device architecture. Applications for write-once–read-many (WORM) memory devices are first demonstrated with a system comprised of gold NPs capped with aromatic thiols that can switch to a stable high-conductivity state, but are unable to switch back to a low-conductivity state. For simplification of the device architecture, two material systems are given that possess easy fabrication and operation. An all-organic system comprised of an electron donor and acceptor yields a highly efficient electrical symbiosis, and, finally, a nanocomposite in which the Au NPs are directly bound to polymer is presented.

4.1. WORM Memory Devices[25,40]

By simply replacing the capping of the Au NPs with conjugated molecules, a WORM device has been demonstrated. This device structure is similar to the polymer-blend system discussed in Section 3, except that Au NPs capped with 2-naphthalenethiol (2NT) (hereafter referred to as Au–2NT NPs) are used to replace the Au NPs capped with saturated alkanethiol.

The device exhibited a very different electrical behavior, and its *I–V* curves are shown in Figure 10a. The current exhibited a rapid increase starting at 4 V at the first voltage scan. It lacks the sudden jump, however. After the voltage scan from 0 to 8 V, the device converted to a high-conductivity state. At 2 V, the current difference in the device between the two conductivity states is different by about three orders of magnitude. Once switched to the high-conductivity state, neither a low nor high voltage bias of either polarity is able to cause the device to revert to the low-conductivity state.

To further understand this electric-field-induced transition, the *I–V* curves in both states were analyzed according to some theoretical models.[41] Before the transition, there is a linear relationship between lg$I$ and $V^{1/2}$ between 0 and 3 V. This suggests that the current before the electrical transition is controlled by charge injection from the Al electrode into the Au–2NT NPs. After the electrical transition, the *I–V* relation changes: lg$I$ has a linear relationship with lg$V$. A best fit of lg$I$–lg$V$ indicates that $I \propto V^{1.9}$. From this it is concluded that the device behavior becomes space-charge-limited.[42]

For devices in the high-conductivity state, the current increases proportionally to the concentration of the Au NPs in the film. This is because both the charge-carrier population and the charge-carrier mobility are dependent on the population of the Au–2NT NPs within the polymer. These results suggest that the Au–2NT NPs are the active media for charge transport through the film because of their conjugated naphthalene structure. This differs from the film of Au–DT NP + 8HQ + PS, where the 8HQ has a conjugated quinoline structure and, thus, becomes the media for charge transfer through the film.

Furthermore, the behavior of these devices suggests an electrical transition due to an electric-field effect, which is evidenced by the fact that the transition voltage increases linearly with the increase in film thickness. This effect can also be identified by the asymmetric *I–V* curve for the device in the high-conductivity state (inset of Fig. 10a), which suggests that the electric field may induce a polarization in the Au–2NT NPs in the polymer film.

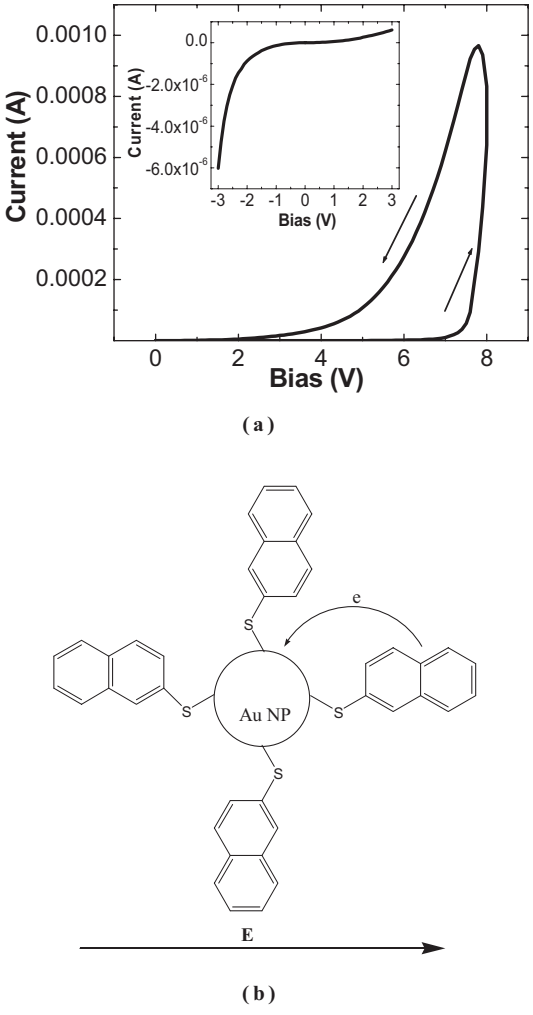

Figure 10. a) *I–V* curves of the device Al/Au–2NT NP + PS/Al. The arrows indicate the voltage-scanning directions. (The inset is the *I–V* curve for the two polarities for the device in the high-conductivity state [40].) b) Schematic of electron transfer from the capping molecule 2NT to the core of the gold NP. Only four 2NT molecules are plotted to represent all capping 2NT molecules on the gold NP. The curved arrow indicates the electron transfer. The straight arrow denotes the direction of the electric field (*E*). Reproduced with permission from [25]. Copyright 2005, IEEE.

Based on these experimental results, we propose an electric-field-induced charge transfer similar to that found in the blended polymer device (Al/Au–DT NP + 8HQ + PS/Al). The polarization of the polymer film after the electronic transition is postulated to be the result of a high electric-field-induced charge transfer between the gold NP and the capping 2NT, where the capping 2NT donates an electron to the core of the gold NP (Fig. 10b). After the charge transfer, the Au–2NT NP polarizes along the applied electric field. Hence, the device will exhibit a higher current when the external electric field is

ADVANCED FUNCTIONAL MATERIALS

applied along this polarization direction than when the field is applied against this polarization.

This model explains the presence of the two conductivity states well. Before the transition, the current is controlled by the charge injection from the electrode into the polymer film due to a big energy barrier between the Al electrode and the Au–2NT NPs. After charge transfer occurs between the Au nanoparticle and 2NT as a result of a high electric field, the 2NT becomes positively charged and the film then exhibits a high current.

4.2. All-Organic Donor–Acceptor Systems

Electrical bistability can also be found in all-organic systems possessing both an electron donor and acceptor.[43] In these systems the electronic-switching mechanism is attributed to an electric-field-induced charge transfer between conjugated organic compounds. In fact, this system presents one of the most direct proofs of this mechanism. This idea is tested by using methanofullerene [6,6]-phenyl C_{61}-butyric acid methyl ester (PCBM) as an organic electron acceptor and tetrathiafulvalene (TTF) as an organic electron donor. The active layer of this device was formed by spin-coating a solution of 1.2 wt % PS, 0.8 wt % TTF, and 0.8 wt % PCBM in 1,2-dichlorobenzene.

The device exhibits electrical bistable behavior, as shown in Figure 11. The voltage to turn the device from a low to high conductivity state is 2.6 V. At this critical voltage, the current increases abruptly from 10^{-7} to 10^{-4} A, and the device is then stable in this high-conductivity state. The low-conductivity state can be recovered by simply applying a larger voltage bias at either polarity (for example, 9 or –9 V can be used) as indicated by curve (c), where the current suddenly drops from

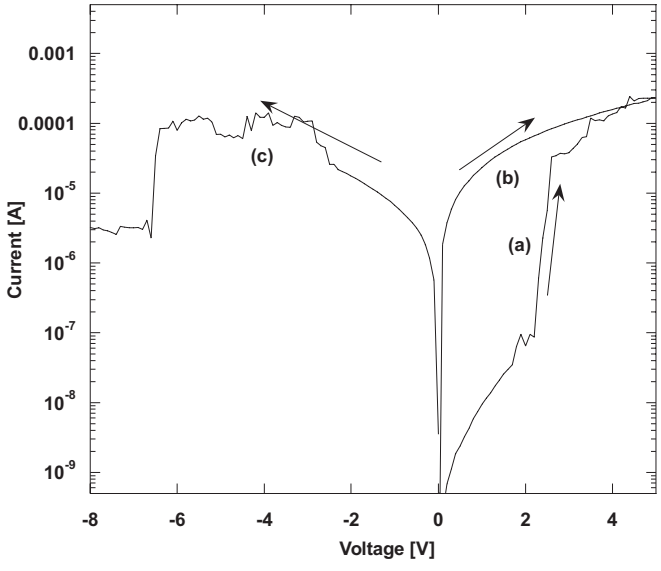

Figure 11. *I–V* curves of the device Al/PS + PCBM + TTF/Al: a) first, b) second, and c) third bias scans. The arrows indicate the voltage-scanning directions. Reproduced with permission from [43].

-10^{-4} to -10^{-6} A at –6.5 V. The switching time for the device from the ON to the OFF or from the OFF to the ON state is shorter than 100 ns.

The stability of these devices was first probed by stress testing. For this experiment, a constant voltage of 0.5 V was applied to the devices while in both the OFF and ON states, and the current output versus time was recorded. It is noted that there was no significant current change for the devices in either state, even after 12 h of continuous stress testing. Stability can also be evaluated by determining the retention ability, which is measured by leaving several devices in the high-conductivity state without any applied voltage in a nitrogen environment. It was witnessed that once the device is in the ON state it will remain that way for several days, sometimes even for weeks. This device can also be successfully cycled between the two states many times, allowing implementation into rewritable memory applications.

To understand the electrical-switching mechanism, we studied the conduction mechanism of the devices in both states. Before the electrical transition, there was a linear relation between log$I$ and $V^{1/2}$ in the voltage range 0–1.7 V. Such linearity suggests that the conduction mechanism is probably thermionic emission,[44] that is, the conduction mechanism is dominated by charge injection. After the electrical transition, a linear relationship was observed between log(I/V) and $V^{1/2}$. Hence, Poole–Frenkel (P–F) emission is probably the conduction mechanism for the device in the high-conductivity state. The P–F conduction mechanism is dominated by charge transport though the bulk materials, which are filled with electrically charged defects.[45] The presence of this P–F mechanism is further confirmed by symmetric *I–V* characteristics for both polarities when using electrodes of dissimilar work functions (i.e., with the ITO/PS + PCBM + TTF/Al configuration). Therefore, the current conduction changes from an injection-dominated mechanism in the OFF state to a charge-transport-dominated mechanism in the ON state.

The switching mechanism was further studied using ac-impedance spectroscopy. The device in the OFF state exhibited a capacitance of 30 pF from 20 to 10^6 Hz, unaffected by changes in frequency. However, when the device was in the ON state, the capacitance became strongly dependent on the frequency. For devices in the ON state, the capacitance in the high-frequency range 10^4–10^6 Hz was almost the same as that in the OFF state, then it subsequently increased with decreasing frequency. The capacitance in the ON state was higher than that in the OFF state by more than one order of magnitude at low frequencies less than 600 Hz. This increased capacitance at low frequency may be influenced by the increase of the apparent dielectric constant of the film. The change of apparent dielectric constant is believed to be associated with the field-induced dipole formation between the donor and acceptor.

In light of the above experimental results and discussions, we propose that the electronic transition is due to an electric-field-induced charge transfer in the film between TTF and PCBM. This can be partially confirmed by observing that the bistable phenomenon does not exist if only one component is present. By noting that the HOMO and LUMO levels for TTF are,

respectively, 5.09 and 2.33 eV,[46] and those for PCBM are, respectively, 6.1 and 3.7 eV,[47] it can be inferred that TTF and PCBM are an electron donor[48] and acceptor,[49] respectively. The materials were chosen because their energy levels do not allow electron transfer in their ground states. Also, the resulting UV-vis absorption spectrum is a superposition of the individual TTF and PCBM spectra. Therefore, the interaction between TTF and PCBM may be weak prior to the electronic transition. In addition, the concentration of charge carriers as a result of impurities in the film is quite low, so that the film has a low conductivity. However, a high electrical field may facilitate electron transfer from the HOMO of TTF to the LUMO of PCBM. Consequently, the HOMO of TTF and LUMO of PCBM become partially filled, and TTF and PCBM are charged positively and negatively, respectively. Therefore, carriers are generated and the device exhibits a sharp increase in conductivity after the charge transfer.

4.3. Polymer with Built-In NP System

By exploiting the advantages of nanocomposite materials, further progress on the development of polymer electronic memory devices can be made.[50] As discussed above, the electrical bistability is related to the electric-field-induced charge transfer between two components. Thus, the compatibility of these two components is crucial for optimal device performance. Enhancing the interface between the two components could lead to superior device performance, and therefore, to this end, a nanocomposite of polyaniline (PANI) nanofibers and Au NPs has been used as the active material.

A conducting polymer (such as PANI) decorated with metallic or semiconducting NPs furnishes an exciting system to investigate, with the prospect of designing device functionality directly into the material. A facile bulk-synthesis method capable of producing high-quality PANI nanofibers, with diameters tunable from 30 to 120 nm, has been employed.[51] The nanocomposite was prepared by growing gold NPs on the PANI nanofibers through the reduction of chloroauric acid ($HAuCl_4$) in an aqueous solution containing the nanofibers.[52] A transmission electron microscopy (TEM) image of the PANI nanofiber/gold NP composite is shown in Figure 12a. An active film was formed by spin-coating an aqueous solution of ~0.1 wt % PANI-nanofiber/gold-NP composite in 1.5 wt % polyvinyl alcohol, with an overall film thickness of 70 nm. Polyvinyl alcohol serves as an electrically insulating matrix for the nanocomposite. The actual device structure and fabrication process are similar to the methods used to fabricate devices with the Al/Au–DT NP + 8HQ + PS/Al system.

This PANI-nanofiber/gold-NP device can be used as an electronic memory device due to its bistable electrical behavior, as seen in Figure 12b. The voltage used to switch the device from the low- to the high-conductivity state is 3 V, where the current changes from 10^{-7} to 10^{-4} A. The device is then stable in the high-conductivity state until a reverse bias of –5 V is applied to return the device to the low-conductivity state. When the voltage is raised above +3 V, a region of negative differential resistance (NDR) is observed, but appears to have no effect on the performance of the device within the +3 to +4 V region. NDR has been reported in other memory devices,[53a,54] and here it seems that this NDR behavior is related to the size of the Au NPs. When the diameters of the gold NPs are greater than 20 nm, the devices can only be switched on once, and during this time in the ON state they exhibit ohmic behavior, indicating that the more metallic nature of larger Au particles dominates the switching. The Au NPs are absolutely critical to the operation of the devices, as devices made with only PANI nanofibers do not demonstrate electronic switching.

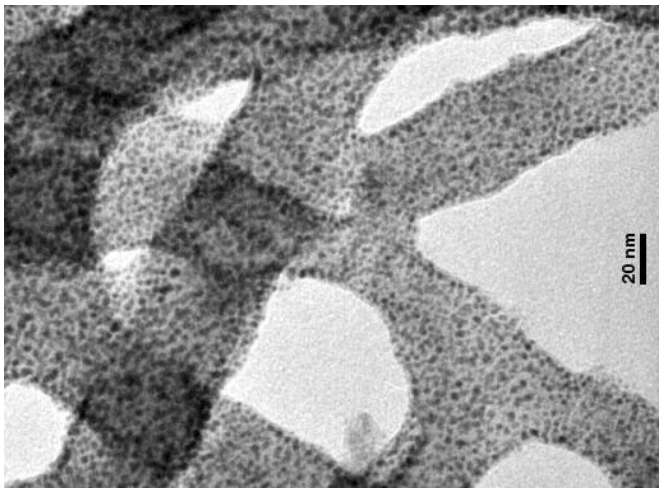

(a)

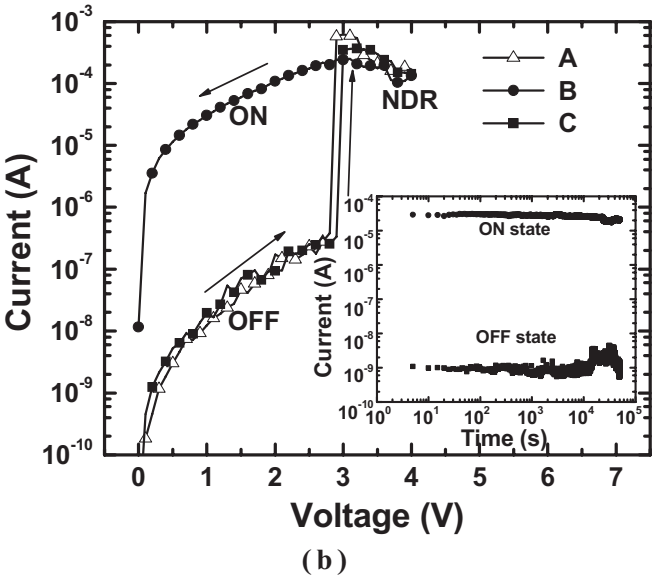

(b)

Figure 12. a) TEM image of the PANI-nanofiber/gold-NP composite. The black dots are ~1 nm gold NPs contained within ~30 nm diameter PANI nanofibers. b) *I–V* curves of the PANI nanofiber/gold-NP device. The potential is scanned from A) 0 to +4 V, B) +4 to 0 V, and C) 0 to +4 V. Between +3 and +4 V a region of negative differential resistance (NDR) is observed. The inset shows the retention-time test of the ON-state (top) and OFF-state (bottom) currents when biased at +1 V every five seconds. Reproduced with permission from [50]. Copyright 2005, American Chemical Society.

ADVANCED FUNCTIONAL MATERIALS

To further demonstrate the feasibility of this material for use as nonvolatile memory, the stability of the system must be evaluated. Data retention was gauged by measuring the current of the device in the ON state over a long period of time, and even after a three-day period no appreciable change in conductivity was observed for these devices. However, after several days, a slight decrease in conductivity in the high-conductivity state was observed. A stress test can indicate the device robustness, and this was performed by applying a constant voltage of 1 V and recording the current every five seconds. In this case, the test occurred over a 14 hour period and ran until the parameter analyzer reached its 10 000 point limit, at which time no significant change in conductivity was witnessed (inset, Fig. 12b).

The PANI-nanofiber/gold-NP device exhibited very fast response times while switching, less than 25 ns for switching ON and OFF. Cycle tests on the device were conducted to measure the lifetimes of the devices, and the parameters used for the write–read–erase voltages are as follows: the write voltage was 4.8 V, the read voltage was 1.2 V, and the erase voltage was –6 V. The current was measured at the read voltage (1.2 V) for the device in the high- and low-conductivity states, and were 10^{-5} A and 10^{-6}–10^{-7} A, respectively. A readily distinguishable ON/OFF ratio around 20 was always maintained.

The switching mechanism in these devices is similar to the all-organic donor–acceptor system discussed in Section 5.2 and appears to be caused by an electric-field charge-transfer effect between the PANI nanofibers and the gold NPs. Under a sufficiently strong electric field, electrons that reside on the imine nitrogen of the PANI may gain enough energy to surmount the interface between the nanofibers and the gold NPs and move onto the gold NPs (Fig. 13). Consequently, the gold NPs become more negatively charged, while the PANI nanofibers become more positively charged. The conductivity of the PANI-nanofiber/gold-NP composite will increase dramatically after the electric-field-induced charge transfer. To corroborate this experimentally, first, X-ray photoelectron spectra taken on the composite showed a shift from 399.2 to 399.7 eV for the N 1s core electrons compared to the undoped, emeraldine base PANI, indicating that the nitrogen in the PANI-nanofiber/gold-NP composite is partially positively charged. At the same time, the binding energy of the gold electrons ($4f_{5/2}$) decreases from 87.7 to 87.5 eV, indicating that a partial negative charge resides on the gold NPs. Second, our assumption of an interface between the PANI nanofibers and gold NPs seems reasonable, since, without such an interface, instability of the device through rapid charge recombination would be expected. Additionally, since our device exhibits NDR, a mechanism involving filament formation is unlikely, as discussed by Scott and coworkers.[53a]

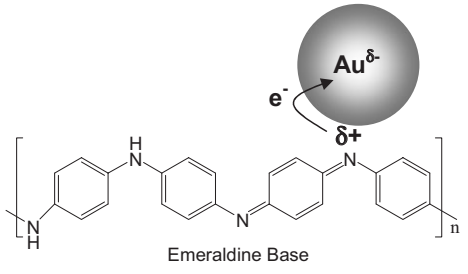

Figure 13. Schematic structure of a PANI-nanofiber/gold-NP after application of +3 V. An increase in charge transfer from PANI to the gold NPs is believed to occur. Reproduced with permission from [50]. Copyright 2005, American Chemical Society.

5. Summary of Polymer/Organic Memory Devices Developed at the University of California, Los Angeles

Though these five devices presented above use different materials, all of them exhibit electrically bistable behavior, and their switching mechanisms are related to the charge storage in their active layers. The charge storage takes place on the metal NPs for the first four devices, while, for the all-organic donor–acceptor device, it takes place on the organic molecules. Charges store in the middle metal-nanocluster layer for the triple-layer devices, and it leads to the polarization of the middle layer. For the three devices made using gold NPs, the charges store on the gold NPs, resulting from an electric-field-induced charge transfer between the gold NPs and conjugated organic compounds or conjugated polymers. The charge storage on the organic compounds, as well as for the all-organic donor–acceptor device, is induced by an external electric field.

6. Research on Polymer/Organic Memory Devices Worldwide

Our research has stimulated strong interest worldwide because of the high potential of using these devices in nonvolatile memory. Devices with different materials or architectures have been demonstrated. The materials used, device architectures, electrical behaviors, and mechanisms of these devices are reviewed in the following paragraphs.

Both small conjugated molecules and polymers were employed as the organic semiconductor materials in these devices. Besides AIDCN presented above, tris-(8-hydroxyquinoline) aluminum (Alq_3),[53a] pentacene,[55] and cyanopolyfluorene[56] were used in the device with a triple-layer structure. Single-layer devices using either small organic compounds or polymers were demonstrated as well. Small organic compounds include pentacene,[55] co-deposited Cu:TCNQ (TCNQ: 7,7,8,8-tetracyanoquinoline),[57] Alq_3,[58] *N*,*N*′-diphenyl-*N*,*N*′-bis(1-naphthyl)-(1,1′-biphenyl)-4,4′-diamine (NPB),[59] poly[3-(6-methoxyhexyl)thiophene],[60,61] and the copolymer of *N*-vinylcarbazole and Eu-complexed vinylbenzoate.[62] Polymers have the advantage of solution processibility. It is still too early to make a correlation between the electronic structure of the materials and device performance, though wide-bandgap organic compounds or polymers may be more favorable.[18,24,63]

These devices exhibit stability in two or multiple conductive states, but the *I*–*V* curves do exhibit discrepancies for different

devices or in different laboratories. Though negative resistance was not observed in our triple-layer devices, it has been observed in some laboratories[53a,64] (Fig. 14). Different dependences of the device performance on film thickness have also been observed. For example, Oyamada et al.[57] found that the

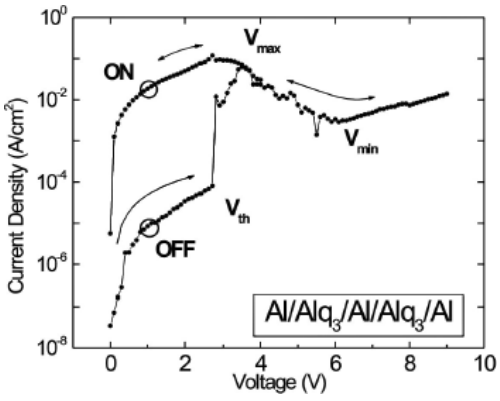

Figure 14. Current–voltage characteristic of an Al/(50 nm)/Alq_3 (50 nm)/Al (5 nm)/Alq_3 (50 nm)/Al (50 nm) device. Reproduced with permission from [53a]. Copyright 2004, American Institute of Physics.

switching characteristics were almost independent of the organic layer, while Tondelier et al.[55] observed that the switching threshold voltage varies approximately linearly with the film thickness. These different behaviors may be attributed to the different parameters for the device fabrication in different laboratories. The electrical behavior of the device is strongly related to the device-fabrication conditions.

The switching mechanism for these devices has been the subject of debate; we propose electric-field-induced polarization of the middle metal layer for the triple-layer devices, and electric-field-induced charge transfer for the polymer version of the single-layer devices. The charge-transfer mechanism is adopted in the devices that use co-deposited Cu:TCNQ[57] or the copolymer of *N*-vinylcarbazole and Eu-complexed vinylbenzoate.[62] In addition to these mechanisms, several different mechanisms have also been proposed. Tondelier et al. studied bistable devices with a single-layer or triple-layer structure, and found similar electrical behavior for both devices.[55] They believed that switching of the device from the low- to the high-conductivity state is the result of the formation of nanofilamentary metallic pathways through the organic film that resulted from field-induced percolation of the metal NPs. However, many other groups disagree with this filament-formation mechanism, and believe that the switching is related to charge storage (either charge transfer or charge trapping) in the metal NPs.

The change of the conductance of the device may be due to the effect of charge storage on the charge injection or charge transport. Bozano et al. interpreted NDR of their device in terms of the Simmons and Verderber (SV) model.[53a] They argued that the switching from high to low conductance is due to charge trapping on the metal NPs and the resulting space-charge field inhibits charge injection. This charge-trapping mechanism was adopted by some other groups as well.[59,65] On the other hand, Tang et al. argued that the SV model may not be a good one for the conductance switching, since it disregards potential energy changes resulting from the charging process.[64] They believe that the electrical behavior in their devices was caused by 2D single-electron tunneling by nanometer-sized metal islands, formed unexpectedly by the nucleation and growth of a metal thin-film electrode. Yet another model was proposed by Rozenberg et al.[66] They proposed three kinds of metal domains in the film between the top and bottom electrodes: the top domain, the middle domain, and the bottom domain (Fig. 15). The current through the two electrodes is controlled by the charge injection into the top or bottom domain, tunneling through the domains, and, finally,

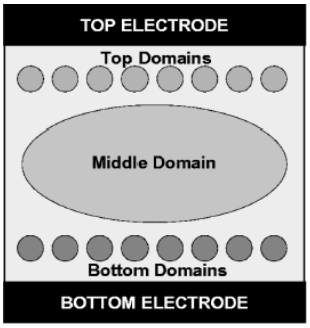

Figure 15. Schematic view of the model with top and bottom electrodes, insulating medium, smaller top and bottom domains, and large middle domains. Reproduced with permission from [66]. Copyright 2004, the American Physical Society.

tunneling to another electrode. The charge tunneling between the bottom (or top) domains and the middle domains is much larger than the tunneling between the bottom (or top) electrode and the bottom (or top) domains. When a voltage produces a large transfer from the middle to the top domain and from the bottom to the middle domain, switching from low to high conductance takes place. On the other hand, when a voltage fills up the bottom domains and empties the top ones, the probability of carrier transfer into the already-filled bottom domains is low and, likewise, the probability of carrier transfer out of the emptied top domains to the electrode is also low. Hence, the device is switched to the low-conductance state. Majumdar et al. thought that the bistability is related to the metal/film interface, and proposed that the space charge stored at the polymer layer near the metal/polymer interface controls charge injection and results in hysteresis-type *I–V* characteristics.[60,61]

Bistable devices that operate by using ion diffusion[67,68] or conformational change of special molecules[69,70] have also been demonstrated. These mechanisms do not involve charge storage at bulk film or at metal/film interface, and therefore these devices were not discussed here.

ADVANCED FUNCTIONAL MATERIALS

7. Summary and Outlook

Electrically addressable bistable devices based on organic and polymer films have been developed for memory applications. Several materials and device structures with bistable states have been reviewed, including the organic/metal-nanocluster/organic structure, polymer composites blended with synthesized metal NPs, polymer nanofibers decorated with NPs, and donor–acceptor complexes. *I–V* characteristics show a conductance change of at least three orders of magnitude. These transitions between the ON and OFF states can be triggered on a nanosecond time scale. The fast response times suggest that the switching is due to electric-field-induced charge transfer. Details of retention time and write–read–erase cycles, pertinent for memory performance, are also provided.

The bistable effect is a fascinating phenomenon covering physics, chemistry, and materials science. The abrupt transition of electrical conductivity on a nanosecond time scale is a quantum phenomenon, although observed in a large-scale device. Although these devices show promising performance, they are still in the early stages of research. Several important issues are still not clear at this moment. For example, how do the size and density of the nanoparticles affect the bistability? Where are the charges stored in the nanoparticles—in their metallic cores or in the bonded molecules? What determines the switching speed and why does the switching voltage vary slightly for different voltage scans? Finally, what are the device-failure mechanisms and what is the ultimate in device performance? These questions are not only important for satisfying scientific interests, but are also important for future practical applications. By resolving these scientific issues, we believe that much more interesting phenomena will be discovered and these organic bistable devices will open a new direction for future organic electronics.

Received: June 16, 2005
Final version: October 16, 2005
Published online: March 14, 2006

[1] R. H. Friend, R. W. Gymer, A. B. Holmes, J. H. Burroughes, R. N. Marks, C. Taliani, D. D. C. Bradley, D. A. Dos Santos, J. L. Brédas, M. Lögdlund, W. R. Salaneck, *Nature* **1999**, *397*, 121.

[2] W. E. Howard, *Sci. Am.* **2004**, *290*, 76.

[3] a) H. Sirringhuas, N. Tessler, R. H. Friend, *Science* **1998**, *280*, 1741. b) C. D. Dimitrakopoulos, D. J. Mascaro, *IBM J. Res. Dev.* **2001**, *45*, 11.

[4] a) G. Yu, J. Gao, J. C. Hummelen, F. Wudl, A. J. Heeger, *Science* **1995**, *270*, 1789. b) C. J. Brabec, N. S. Sariciftci, J. C. Hummelen, *Adv. Funct. Mater.* **2001**, *11*, 15.

[5] a) K. Nakayama, K. Kojima, Y. Imai, T. Kasai, S. Fukushima, A. Kitagawa, M. Kumeda, Y. Kakimoto, M. Suzuki, *Jpn. J. Appl. Phys., Part 1* **2003**, *42*, 404. b) J. F. Dewald, A. D. Pearson, W. R. Northover, J. Peck, *J. Electrochem. Soc.* **1962**, *109*, 243c. c) H. J. Hovel, J. J. Urgell, *J. Appl. Phys.* **1971**, *42*, 5076.

[6] a) M. Mitkova, M. N. Kozicki, *J. Non-Cryst. Solids* **2002**, *299–302*, 1023. b) M. N. Kozicki, W. C. West, *US Patent 5 761 115*, **1998**.

[7] a) T. Rueckes, K. Kim, E. Joselevich, G. Y. Tseng, C. L. Cheung, C. M. Lieber, *Science* **2000**, *289*, 94. b) R. L. Badzey, G. Zolfagharkhani, A. Gaidarzhy, P. Mohanty, *Appl. Phys. Lett.* **2005**, *86*, 23 106.

[8] K. Terabe, T. Hasegawa, T. Nakayama, M. Aono, *Nature* **2005**, *433*, 47.

[9] a) N. Kouklin, S. Bandyopadhyay, S. Tereshin, A. Varfolomeev, D. Zaretsky, *Appl. Phys. Lett.* **2000**, *76*, 460. b) R. Ohab, N. Sugiyama, K. Uchida, J. Koga, A. Toriumi, *IEEE Trans. Electron Devices* **2002**, *49*, 1392.

[10] a) K. W. Guarini, C. T. Black, Y. Zhang, I. V. Babich, E. M. Sikorski, L. M. Gignac, *IEEE Int. Electron Device Meet., Tech. Dig.* **2003**, 541. b) M. L. Ostraat, J. W. De Blauwe, M. L. Green, L. D. Bell, M. L. Brongerma, J. R. Casperson, C. Flagan, H. A. Atwater, *Appl. Phys. Lett.* **2001**, *79*, 433.

[11] a) J. C. Scott, *Science* **2004**, *304*, 62. b) K. S. Kwok, J. C. Ellenbogen, *Mater. Today* **2002**, *5*, 28.

[12] A. S. Blum, J. G. Kushmerick, D. P. Long, C. H. Patterson, J. C. Yang, J. C. Henderson, Y. Yao, J. M. Tour, R. Shashidhar, B. R. Ratna, *Nat. Mater.* **2005**, *4*, 167.

[13] Y. Chen, G. Y. Jung, D. A. A. Ohlberg, X. Li, D. R. Stewart, J. O. Jeppesen, K. A. Nielsen, J. F. Stoddart, R. S. Williams, *Nanotechnology* **2003**, *14*, 462.

[14] a) K. Okamoto, Y. Araki, O. Ito, S. Fukuzumi, *J. Am. Chem. Soc.* **2004**, *126*, 56. b) B. I. Ipe, K. G. Thomas, S. Barazzouk, S. Hotchandani, P. V. Kamat, *J. Phys. Chem. B* **2002**, *106*, 18.

[15] H. Peng, C. Ran, X. Yu, R. Zhang, Z. Liu, *Adv. Mater.* **2005**, *17*, 459.

[16] L. P. Ma, J. Liu, S. Pyo, Y. Yang, *Appl. Phys. Lett.* **2002**, *80*, 362.

[17] a) R. Schroeder, L. A. Majewski, M. Grell, *Adv. Mater.* **2004**, *16*, 633. b) S. Kolliopoulou, P. Dimitrakis, P. Normand, H. L. Zhang, N. Cant, S. D. Evans, S. Paul, C. Pearson, A. Molloy, M. C. Petty, D. Tsoukalas, *J. Appl. Phys.* **2003**, *94*, 5234.

[18] a) L. P. Ma, J. Liu, Y. Yang, *US patent application, US 01/17 206*, **2001**. b) L. P. Ma, J. Liu, Y. Yang, *Appl. Phys. Lett.* **2002**, *80*, 2997. c) L. P. Ma, S. M. Pyo, J. Ouyang, Q. F. Xu, Y. Yang, *Appl. Phys. Lett.* **2003**, *82*, 1419.

[19] Y. Yang, L. P. Ma, J. Wu, *MRS Bull.* **2004**, *29*, 833.

[20] L. P. Ma, J. Liu, S. M. Pyo, Q. F. Xu, Y. Yang, *Molec. Cryst. Liq. Cryst.* **2002**, *378*, 185.

[21] a) J. F. Kwak, G. Beni, P. M. Chaikin, *Phys. Rev. B* **1976**, *13*, 641. b) M. Ulmke, R. T. Scalettar, A. Nazarenko, E. Dagotto, *Phys. Rev. B* **1996**, *54*, 16 523.

[22] J. H. Wu, L. P. Ma, Y. Yang, *Phys. Rev. B* **2004**, *69*, 11 531.

[23] J. He, L. P. Ma, J. Wu, Y. Yang, *J. Appl. Phys.* **2005**, *97*, 64 507.

[24] J. Ouyang, C. W. Chu, C. R. Szmanda, L. P. Ma, Y. Yang, *Nat. Mater.* **2004**, *3*, 918.

[25] J. Ouyang, C. W. Chu, R. J. Tseng, A. Prakash, Y. Yang, *Proc. IEEE* **2005**, *93*, 1287.

[26] M. J. Hostetler, J. E. Wingate, C. J. Zhong, J. E. Harris, R. W. Vachet, M. R. Clark, J. D. Londono, S. J. Green, J. J. Stokes, G. D. Wignall, G. L. Glish, M. D. Porter, N. D. Evans, R. W. Murray, *Langmuir* **1998**, *14*, 17.

[27] W. Wang, T. Lee, M. A. Reed, *Phys. Rev. B* **2003**, *68*, 035 416.

[28] Y. Chen, D. A. A. Ohlberg, X. Li, D. R. Stewart, R. S. Williams, J. O. Jeppesen, K. A. Nielsen, J. F. Stoddart, D. L. Olynick, E. Anderson, *Appl. Phys. Lett.* **2003**, *82*, 1610.

[29] T. Tsujioka, H. Kondo, *Appl. Phys. Lett.* **2003**, *83*, 937.

[30] a) M. N. Kozicki, M. Yun, S. J. Yang, J. P. Aberouette, J. P. Bird, *Superlattices Microstruct.* **2000**, *27*, 485. b) A. E. Owen, P. G. Le Comber, J. Hajto, M. J. Rose, A. J. Snell, *Int. J. Electron.* **1992**, *73*, 897. c) H. Pagnia, N. Sotnik, *Phys. Status Solidi A* **1988**, *108*, 11.

[31] H. Carchano, R. Lacoste, Y. Segui, *Appl. Phys. Lett.* **1971**, *19*, 414.

[32] a) C. K. Prout, A. G. Wheeler, *J. Chem. Soc. A* **1967**, 469. b) E. Castellano, C. K. Prout, *J. Chem. Soc. A* **1971**, 550.

[33] a) D. M. Adams, L. Brus, C. E. D. Chidsey, S. Creager, C. Creutz, C. R. Kagan, P. V. Kamat, M. Lieberman, S. Lindsay, R. A. Marcus, R. M. Metzger, M. E. Michel-Beyerle, J. R. Miller, M. D. Newton, D. R. Rolison, O. Sankey, K. S. Schanze, J. Yardley, X. Y. Zhu, *J. Phys. Chem. B* **2003**, *107*, 6668. b) B. I. Ipe, K. G. Thomas, S. Barazzouk, S. Hotchandani, P. V. Kamat, *J. Phys. Chem. B* **2002**, *106*, 18.

[34] X.-L. Mo, G.-R. Chen, Q.-J. Cai, Z.-Y. Fan, H.-H. Xu, Y. Yao, J. Yang, H.-H. Gu, Z.-Y. Hua, *Thin Solid Films* **2003**, *436*, 259.

[35] a) T. Furukawa, *Adv. Colloid Interface Sci.* **1997**, *71–72*, 183. b) L. Jie, E. Schreck, K. Dransfeld, *Appl. Phys. A* **1991**, *53*, 457.

[36] a) S. Chen, R. S. Ingram, M. J. Hostetler, J. J. Pietron, R. W. Murray, T. G. Schaaff, J. T. Khoury, M. M. Alvarez, R. L. Whetten, *Science* **1998**, *280*, 2098. b) J. F. Hicks, A. C. Templeton, S. W. Chen, K. M. Sheran, R. Jasti, R. W. Murray, J. Debord, T. G. Schaaf, R. L. Whetten, *Anal. Chem.* **1999**, *71*, 3703.
[37] *Gaussian 03*, *Revision B.05*, Gaussian, Inc., Pittsburgh, PA **2003**.
[38] R. Kubo, *J. Phys. Soc. Jpn.* **1962**, *17*, 975.
[39] S. Chen, R. W. Murray, S. W. Feldberg, *J. Phys. Chem. B* **1998**, *102*, 9898.
[40] J. Ouyang, C. W. Chu, D. Sievers, Y. Yang, *Appl. Phys. Lett.* **2005**, *86*, 123 507.
[41] W. Brütting, S. Berleb, A. G. Mückl, *Org. Electron.* **2001**, *2*, 1.
[42] D. Braun, *J. Polym. Sci. Part B* **2003**, *41*, 2622.
[43] C. W. Chu, J. Ouyang, J. H. Tseng, Y. Yang, *Adv. Mater.* **2005**, *17*, 1440.
[44] E. H. Rhoderick, R. H. Williams, *Metal-Semiconductor Contacts*, Clarendon Press, Oxford **1988**.
[45] a) C. Laurent, E. Kay, *J. Appl. Phys.* **1988**, *64*, 336. b) W. Vollmann, H. U. Poll, *Thin Solid Films* **1975**, *26*, 201.
[46] N. Martín, E. Ortí, L. Sánchez, P. M. Viruela, R. Viruela, *Eur. J. Org. Chem.* **1999**, 1239.
[47] C. J. Brabec, N. S. Sariciftci, J. C. Hummelen, *Adv. Funct. Mater.* **2001**, *11*, 15.
[48] a) M. R. Bryce, *Adv. Mater.* **1999**, *11*, 11. b) J. Ferrais, D. O. Cowan, V. Walatka, J. H. Perlstein, *J. Am. Chem. Soc.* **1972**, *95*, 948.
[49] L. Zheng, Q. Zhou, X. Deng, M. Yuan, G. Yu, Y. Cao, *J. Phys. Chem. B* **2004**, *108*, 11 921.
[50] R. J. Tseng, J. Huang, J. Ouyang, R. B. Kaner, Y. Yang, *Nano Lett.* **2005**, *5*, 1077.
[51] a) J. Huang, S. Virji, B. H. Weiller, R. B. Kaner, *J. Am. Chem. Soc.* **2003**, *125*, 314. b) J. Huang, R. B. Kaner, *J. Am. Chem. Soc.* **2004**, *126*, 851. c) S. Virji, J. Huang, R. B. Kaner, B. H. Weiller, *Nano Lett.* **2004**, *4*, 491.
[52] a) J. Huang, S. Virji, B. H. Weiller, R. B. Kaner, *Chem. Eur. J.* **2004**, *10*, 1314. b) J. Wang, K. G. Neoh, E. T. Kang, *J. Colloid Interface Sci.* **2001**, *239*, 78. c) J. A. Smith, M. Josowicz, J. Janata, *J. Electrochem. Soc.* **2003**, *150*, E384.
[53] a) L. D. Bozano, B. W. Kean, V. R. Deline, J. R. Salem, J. C. Scott, *Appl. Phys. Lett.* **2004**, *84*, 607. b) M. Beinhoff, L. D. Bozano, J. C. Scott, K. R. Carter, *Polym. Mater. Sci. Eng.* **2004**, *90*, 211.
[54] a) J. D. Le, Y. He, T. R. Hoye, C. C. Mead, R. A. Kiehl, *Appl. Phys. Lett.* **2003**, *83*, 5518. b) J. Chen, J. Su, W. Wang, M. A. Reed, *Phys. E* **2003**, *16*, 17.
[55] D. Tondelier, K. Lmimouni, D. Vuillaume, C. Fery, G. Haas, *Appl. Phys. Lett.* **2004**, *85*, 5763.
[56] T. Ouisse, O. Stéphan, *Org. Electron.* **2004**, *5*, 251.
[57] T. Oyamada, H. Tanaka, K. Matsushige, H. Sasabe, C. Adachi, *Appl. Phys. Lett.* **2003**, *83*, 1252.
[58] A. K. Mahapatro, R. Agrawal, S. Ghosh, *J. Appl. Phys.* **2004**, *96*, 3583.
[59] J. Chen, D. Ma, *Appl. Phys. Lett.* **2005**, *87*, 023 505.
[60] H. S. Majumdar, A. Bandyopadhyay, *J. Appl. Phys.* **2002**, *91*, 2433.
[61] H. S. Majumdar, A. Bolognesi, A. J. Pal, *Synth. Met.* **2004**, *140*, 203.
[62] Q. Ling, Y. Song, S. J. Ding, C. Zhu, D. S. H. Chan, D.-L. Kwong, E.-T. Kang, K.-G. Neoh, *Adv. Mater.* **2005**, *17*, 455.
[63] M. Beinhoff, L. D. Bozano, J. C. Scott, K. R. Carter, *Macromolecules* **2005**, *38*, 4147.
[64] W. Tang, H. Shi, G. Xu, B. S. Ong, Z. D. Popovic, J. Deng, J. Zhao, G. Rao, *Adv. Mater.* **2005**, *17*, 2307.
[65] S. H. Kang, T. Crisp, I. Kymissis, V. Bulovic, *Appl. Phys. Lett.* **2004**, *85*, 4666.
[66] M. J. Rozenberg, J. H. Inoue, M. J. Sánchez, *Phys. Rev. Lett.* **2004**, *92*, 178 302.
[67] L. Ma, Q. Xu, Y. Yang, *Appl. Phys. Lett.* **2004**, *84*, 4908.
[68] J. H. A. Smits, S. C. J. Meskers, R. A. J. Janssen, A. W. Marsman, D. M. de Leeuw, *Adv. Mater.* **2005**, *17*, 1169.
[69] A. Bandyopadhyay, A. J. Pal, *J. Phys. Chem. B* **2003**, *107*, 2531.
[70] A. Bandyopadhyay, A. J. Pal, *J. Phys. Chem. B* **2005**, *109*, 6084.